

# Direct observation of a pure focused evanescent field of a high numerical aperture objective lens by scanning near-field optical microscopy

Baohua Jia, Xiaosong Gan,<sup>a)</sup> and Min Gu

Centre for Micro-Photonics, Faculty of Engineering and Industrial Sciences, Swinburne University of Technology, P.O. Box 218 Hawthorn, 3122 Australia

(Received 4 October 2004; accepted 15 February 2005; published online 22 March 2005)

Intensity distributions of a tightly focused evanescent field generated by a center blocked high numerical aperture (1.65) objective lens are investigated by a scanning near-field optical microscope. The pure focused evanescent field is mapped and a splitting phenomenon of the focal spot along the direction of polarization, caused by depolarization, is observed not only on the interface, where the evanescent field is generated, but also in the parallel planes away from the interface. The decaying nature of the focused evanescent field shows good agreement with the theoretical predication, indicating that the field is purely evanescent and does not contain a significant contribution from the propagating component. It is found in our experiment that the light coupling efficiencies of the longitudinal polarization component  $E_z$  and the transverse polarization component  $E_x$  to the fiber probe differ by a factor of 3. © 2005 American Institute of Physics. [DOI: 10.1063/1.1886250]

A focused evanescent field generated by a high numerical aperture (NA) objective under total internal reflection (TIR) provides a unique tool for studying light-matter interaction at the single-molecule level because of its high resolution in all spatial dimensions.<sup>1-9</sup> This technique combines the advantages of a high NA objective, which provides high lateral resolution, and the evanescent nature of TIR, which confines the light within one-tenth of the wavelength from the interface. Such properties are highly desirable for many applications, including near-field two-photon excitation<sup>7</sup> and near-field trapping, in which the fast decaying nature of the evanescent field can shrink the axial size to approximately 60 nm, therefore reducing the excitation or trapping volume significantly.<sup>9</sup> On the other hand, in microscopy imaging, the evanescent field generated by TIR can suppress the background noise and improve the contrast of the image dramatically, thus allowing the observation of the dynamics of single-molecule reactions *in vivo*.<sup>10-12</sup> It is noted that the tightly focused laser light by a high NA objective lens exhibits some special characteristics in the focal region, such as the focus elongation due to the presence of the longitudinal polarization component.<sup>13,14</sup> Such a phenomenon becomes more pronounced when the field becomes purely evanescent. The completed knowledge of a pure focused evanescent field, particularly its polarization states, is a prerequisite for a wide range of applications including single-molecule detection,<sup>1-4,10-12,15</sup> Raman spectroscopy,<sup>5</sup> near-field nonlinear imaging,<sup>6-8</sup> and near-field trapping.<sup>9</sup>

Experimental characterizations of a focused evanescent field have been attempted with small pointlike objects, such as single molecules<sup>4</sup> or nanocrystals.<sup>7</sup> However, such measurements rely on the fluorescence excitation or other type of indirect reflection of the optical field and a low signal-to-noise ratio is often the problem associated with these probes. In addition, using pointlike objects only allows the characterization at the interface, where an evanescent field is generated. Mapping of a tightly focused spot has also been

achieved by using a scanning near-field optical microscope (SNOM) with dielectric or metallic probes.<sup>16-19</sup> However, such investigations are conducted with contributions from both the propagating and evanescent components, in which case the light confinement in the close vicinity of an interface was not realized.

In this letter, we demonstrate the direct mapping of a pure focused evanescent field generated by an annular beam illuminated high NA objective (NA=1.65) using a SNOM with a metallic-coated fiber tip. The focus splitting phenomenon has been observed. In particular, the pure focused evanescent field is mapped in a series of planes with different distances from the glass-air interface and the fast decaying nature of the field is also demonstrated. All experimental measurements match well with the theoretical calculations using vectorial diffraction theory.<sup>20-23</sup>

A schematic diagram of the experimental setup is shown in Fig. 1(a). A linearly polarized He-Ne laser beam is coupled into a high NA objective (Olympus, NA=1.65, 100×). A confocal pinhole, located in front of a photomultiplier tube at the detection arm provides optical sectioning properties and is used to ensure that the center of the focal spot is placed at the glass-air interface. A SNOM head (NT-MDT) with a fiber probe vertical to the interface is placed on top of a cover glass. The tightly focused field is directly mapped with the fiber probe scanning in a transverse plane parallel to the interface [Fig. 1(b)]. An aluminium-coated probe with an aperture of 30–100 nm in diameter is used for measurements. During the experiment, the distance between the tip and the cover glass surface is controlled by the shear force mechanism. The mapping of a focal spot produced by an unobstructed objective is shown in Fig. 1(c). It is noted that the focal spot is elongated along the direction of polarization, which has been predicted by the theoretical calculation<sup>20-23</sup> and confirmed by other experimental measurements.<sup>7,8,13,14</sup> The full width at half maximum of the spot in the directions parallel and perpendicular to the polarization direction is approximately 420 nm and 275 nm, respectively, which are comparable to the theoretical values,

<sup>a)</sup>Electronic mail: xgan@swin.edu.au

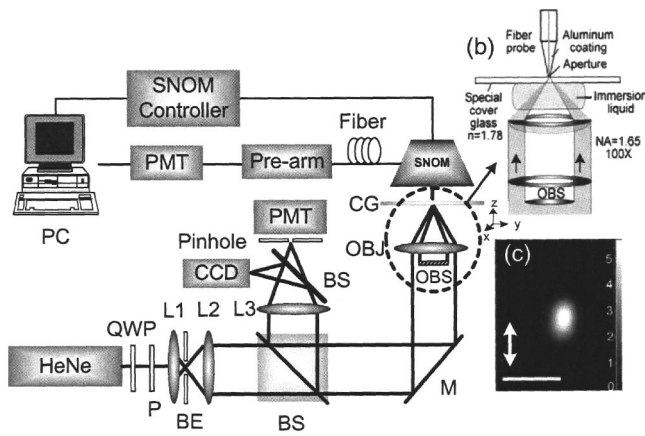


FIG. 1. (a) A schematic diagram of the experimental setup for mapping a focused evanescent field using a SNOM. QWP: quarter wave plate, P: polarizer, BE: beam expansion system, BS: beam splitter, M: mirror, L1, L2, L3: lenses, OBJ: objective, NA=1.65, 100 $\times$ , OBS: obstruction. Insert (b); Schematic of the generation of a focused evanescent field and the detection using a SNOM probe. Insert (c); The mapping of the intensity distribution in the focal region at the glass-air interface under circular illumination ( $\epsilon=0$ ). The arrow denotes the direction of polarization of the illumination. Scale bar: 500 nm.

400 nm and 250 nm, respectively. It should be pointed out that the electric field at the interface is mixed with both propagating and evanescent components, which have substantial differences in their characteristics. In order to obtain a thorough understanding of a pure focused evanescent field, it is required to isolate it from the propagating component.

For this purpose, an obstruction disk with a size larger than the critical radius  $\epsilon_c$  (corresponding to the critical angle and normalized by the back aperture radius of the objective, for example,  $\epsilon_c=0.6$  for a glass-air interface) is inserted in the illumination path as close as possible to the back aperture of the objective, as shown in Fig. 1(b), to produce a pure focused evanescent field. In our experiments, the obstruction disk has a normalized radius of  $\epsilon=0.803$ , which is much larger than the critical radius; therefore physically, the measurement is free of all the propagating components. The mapping of the intensity distributions in the transverse planes of different distances to the interface is shown in Fig. 2. It can be clearly seen that the intensity of the focused evanescent field has two identifiable peaks in the direction of the incident polarization. It should be pointed out that one of the advantages of using a fiber probe rather than pointlike objects, such as single molecules<sup>4</sup> or quantum dots,<sup>7</sup> is that the electric field can be mapped three dimensionally. As an example, the intensity distributions at the planes parallel to the interface with distances of 10 nm, 20 nm, 40 nm, and 500 nm are presented in Figs. 2(b)–2(e). The first feature that is noticeable in these measurements is that the peak intensity

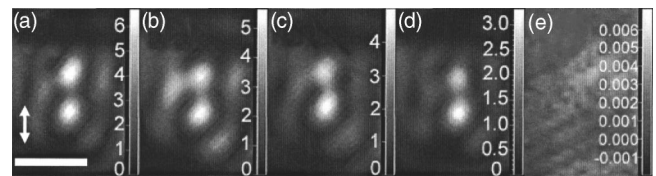


FIG. 2. Measured intensity distributions of pure evanescent focuses at the horizontal planes of different distances  $d$  to the glass-air interface ( $\epsilon=0.803$ ): (a) At interface, (b)  $d=10$  nm, (c)  $d=20$  nm, (d)  $d=40$  nm, and (e)  $d=500$  nm. The arrow denotes the direction of polarization of the illumination. Scale bar: 500 nm.

distributions in the focal region show a pronounced drop from 6.5 [Fig. 2(a)] to nearly 0 [Fig. 2(e)], as is indicated by the intensity bar on the right hand of each figure (the intensity of each figure has been normalized by its maximum). This decaying nature is confirmed by plotting the measured intensity at one of the peak intensity spots as a function of the distance between the probe and the interface [Fig. 3(a)]. It is demonstrated that the pure focused evanescent field decays exponentially and the decay constant is estimated to be 54 nm, which has a reasonable agreement with the theoretical prediction (48 nm) for the total intensity distribution rather than any other field components.

The calculated cross sections based on the vectorial diffraction theory<sup>20–23</sup> along the illumination polarization direction of the intensity distribution  $|E|^2$ , together with the contributions from the transverse  $|E_x|^2$  and longitudinal polarization component  $|E_z|^2$ , for a ring beam illumination ( $\epsilon=0.803$ ) at a glass-air interface is shown in Fig. 3(b). The transverse component  $|E_y|^2$  is not shown, because it is orders weaker than the other two components. For comparison, the cross section of the measured intensity distribution at the interface is shown in Fig. 4(a). The focus splitting in the direction of illumination polarization can be seen in the measurement. However, the dip at the center is more pronounced than the theoretical prediction shown in Fig. 3(b). One important factor that has been neglected in the discussions so far is the coupling efficiency of different polarization components to the probe. As has been demonstrated before, a metallic probe can enhance the coupling of the longitudinal polarization component  $|E_z|^2$  by orders of magnitude,<sup>17</sup> which results in the inability of detecting the transverse polarization component  $|E_x|^2$ . Similarly, the aluminium coating of the fiber tip used in our experiments also facilitates the enhancement of the longitudinal component  $|E_z|^2$  due to the surface plasmon effect. As a result, the detected field is dominated more by the longitudinal component. Comparing the theoretical field distributions with the experimental data, we found that the theoretical cross sections can be modified by the coupling ratio  $\alpha$  between the coupling efficiencies for

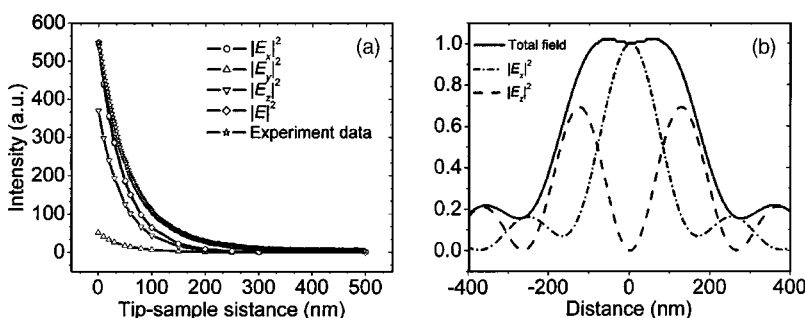


FIG. 3. (a) Experimental and theoretical ( $|E|^2$ ,  $|E_x|^2$ ,  $|E_y|^2$ , and  $|E_z|^2$ ) intensity decay of pure evanescent focuses as a function of the tip-sample distance for  $\epsilon=0.803$ . (b) Calculated cross-sectional distributions of a focused evanescent field  $|E|^2$ , the transverse component  $|E_x|^2$  and longitudinal component  $|E_z|^2$  along the input polarization direction for  $\epsilon=0.803$ .

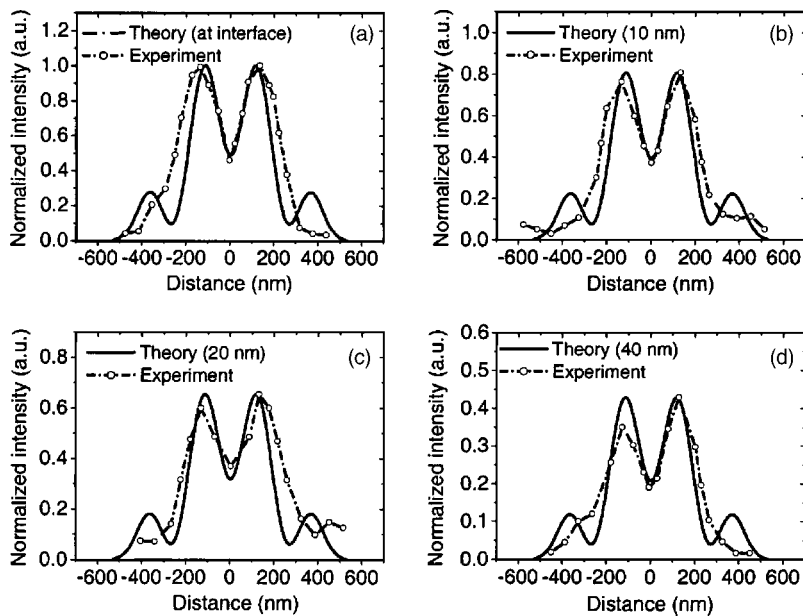


FIG. 4. Comparison of the experimental cross sections with the modified theoretical cross sections along the illumination polarization direction of a pure focused evanescent field for  $\epsilon=0.803$  at the horizontal planes of different distances  $d$  to the glass-air interface detected by a finite size fiber probe (60 nm on average): (a) At interface, (b)  $d=10$  nm, (c)  $d=20$  nm, and (d)  $d=40$  nm.

the longitudinal component and that for the transverse component:  $|E_{\text{detect}}|^2 \approx |E_x|^2 + \alpha|E_z|^2$ . By fitting the experimental intensity value of the middle dip to the theoretical calculation, we obtain the coupling ratio, which is approximately 3.

The finite size of a probe is another factor that needs to be considered in the mapping of a focused electric field. Although most of the near-field probes are tens of nanometers to one hundred nanometers in size, it still cannot be neglected considering that the evanescent focal spots to be mapped are only a few times larger than the probes. The intensity distribution of the evanescent focus mapped by a finite sized probe can be approximated to the convolution of the aperture function of the probe and the calculated focal spot. After taking the coupling efficiencies and the finite probe sizes (60 nm on average) into consideration, the modified theoretical cross-sectional intensity distribution has good agreement with the experimental measurement [Fig. 4(a)]. The distance between the two intensity peaks is 260 nm in the experiment, which is close to the theoretical prediction (235 nm). It should be pointed out that such good agreement is not only demonstrated for the field at the interface, but also at the parallel planes away from the interface [Figs. 4(b)–4(d)], in which case the same ratio of  $\alpha=3$  obtained from the case where the probe is on the surface has been used for all the theoretical estimations. In other words, a good match between the theory and the experiments has been demonstrated in a three-dimensional mapping of a pure focused evanescent field [Figs. 4(b)–4(d)].

In conclusion, the intensity distributions of a pure focused evanescent field produced by a center blocked high NA objective lens have been mapped three dimensionally by using a SNOM. Its decaying nature has been investigated and the measured decay constant shows good agreement with the theoretical prediction, indicating that the field is purely evanescent and does not contain a contribution from the propagating component. Focus splitting along the direction of polarization has also been observed. It has been demonstrated that the light coupling efficiency of the longitudinal

polarization component  $E_z$  is approximately three times that of the transverse polarization component  $E_x$  in our experiment. After taking into consideration the finite size of the fiber probes and different coupling efficiencies between different field components, the experimental measurements quantitatively match the theoretical prediction.

The authors thank the Australian Research Council for its support.

- <sup>1</sup>J. J. Macklin, J. K. Trautman, T. D. Harris, and L. E. Brus, *Science* **272**, 255 (1996).
- <sup>2</sup>R. M. Dickson, D. J. Norris, and W. E. Moerner, *Phys. Rev. Lett.* **81**, 5322 (1998).
- <sup>3</sup>M. Tokunaga, K. Kitamura, K. Saito, A. H. Iwane, and T. Yanagida, *Biochem. Biophys. Res. Commun.* **235**, 47 (1997).
- <sup>4</sup>B. Sick, B. Hecht, and L. Novotny, *Phys. Rev. Lett.* **85**, 4482 (2000).
- <sup>5</sup>N. Hayazawa, A. Tarun, Y. Inouye, and S. Kawata, *J. Appl. Phys.* **92**, 6983 (2002).
- <sup>6</sup>N. Hayazawa, Y. Inouye, and S. Kawata, *J. Microsc.* **194**, 472 (1999).
- <sup>7</sup>J. W. M. Chon, M. Gu, C. Bullen, and P. Mulvaney, *Opt. Lett.* **28**, 1930 (2003).
- <sup>8</sup>K. Bahlmann and S. W. Hell, *J. Microsc.* **200**, 59 (2000).
- <sup>9</sup>M. Gu, J.-B. Haumonte, Y. Micheau, J. W. M. Chon, and X. Gan, *Appl. Phys. Lett.* **84**, 4236 (2004).
- <sup>10</sup>T. Funatsu, Y. Harada, M. Tokunaga, K. Saito, and T. Yanagida, *Nature (London)* **374**, 555 (1995).
- <sup>11</sup>A. Ishijima and T. Yanagida, *Trends Biochem. Sci.* **26**, 438 (2001).
- <sup>12</sup>Y. Sako and T. Uyemura, *Cell Struct. Funct.* **27**, 205 (2002).
- <sup>13</sup>K. Bahlmann and S. W. Hell, *Appl. Phys. Lett.* **77**, 612 (2000).
- <sup>14</sup>R. Dorn, S. Quabis, and G. Leuchs, *J. Mod. Opt.* **50**, 1917 (2003).
- <sup>15</sup>T. Ha, T. Enderle, and D. S. Chemla, *Phys. Rev. Lett.* **77**, 3979 (1996).
- <sup>16</sup>S. K. Rhodes, K. A. Nugent, and A. Robers, *J. Opt. Soc. Am. A* **19**, 1689 (2002).
- <sup>17</sup>A. Bouhelier, M. Beversluis, A. Hartschuh, and L. Novotny, *Phys. Rev. Lett.* **90**, 013903 (2003).
- <sup>18</sup>Y. H. Fu, F. H. Ho, W.-C. Lin, W. C. Liu, and D. P. Tsai, *J. Microsc.* **210**, 225 (2003).
- <sup>19</sup>Y. H. Fu, W.-C. Liu, and D. P. Tsai, *Scanning* **26**, 52 (2004).
- <sup>20</sup>B. Richards and E. Wolf, *Proc. R. Soc. London, Ser. A* **253**, 358 (1959).
- <sup>21</sup>C. J. R. Sheppard, *Optik (Stuttgart)* **48**, 329 (1977).
- <sup>22</sup>P. Torok, P. Varga, Z. Laczik, and G. R. Booker, *J. Opt. Soc. Am. A* **12**, 325 (1995).
- <sup>23</sup>M. Gu, *Advanced Optical Imaging Theory* (Springer, Heidelberg, 2000).